nature portfolio

https://doi.org/10.1038/s41586-024-07136-2

Supplementary information

All-optical frequency division on-chip using a single laser

In the format provided by the
authors and unedited

All-optical frequency division on-chip using a single laser: supplementary material

Yun Zhao,[1,2] Jae K. Jang,[1] Garrett J. Beals,[1] Karl J. McNulty,[2] Xingchen Ji,[2] Yoshitomo Okawachi,[1] Michal Lipson,[2,1] and Alexander L. Gaeta[1,2,*]

[1]*Department of Applied Physics and Applied Mathematics, Columbia University, New York, NY 10027, USA*
[2]*Department of Electrical Engineering, Columbia University, New York, NY 10027, USA*

(Dated: December 22, 2023)

Supplementary material for "All-optical frequency division on-chip using a single laser."

I. SCHAWLOW-TOWNES LINEWIDTH OF $\chi^{(3)}$-BASED OPO

The Schawlow-Townes linewidth (STL) represents the fundamental linewidth of an optical oscillator, which is induced by the quantum fluctuations of related fields. Due to the extremely low occupation number of thermal photons at room temperatures, the only quantum fluctuations contributing to the STL of an OPO are vacuum fluctuations. The $\chi^{(3)}$-based OPO process with vacuum fluctuations can be modeled as,

$$\frac{d\hat{A}}{dt} = -\frac{\alpha}{2}\hat{A} - i\Delta_A\hat{A} + i\Gamma(\hat{A}^\dagger\hat{A} + 2\hat{B}^\dagger\hat{B} + 2\hat{C}^\dagger\hat{C})\hat{A} + i2\Gamma\hat{A}^\dagger\hat{B}\hat{C} + \sqrt{\kappa}A_{\text{in}} + \sqrt{\alpha}\hat{a}_{\text{in}}, \tag{1}$$

$$\frac{d\hat{B}}{dt} = -\frac{\alpha}{2}\hat{B} - i\Delta_B\hat{B} + i\Gamma(2\hat{A}^\dagger\hat{A} + \hat{B}^\dagger\hat{B} + 2\hat{C}^\dagger\hat{C})\hat{B} + i\Gamma\hat{C}^\dagger\hat{A}^2 + \sqrt{\alpha}\hat{b}_{\text{in}}, \tag{2}$$

$$\frac{d\hat{C}}{dt} = -\frac{\alpha}{2}\hat{C} - i\Delta_C\hat{C} + i\Gamma(2\hat{A}^\dagger\hat{A} + 2\hat{B}^\dagger\hat{B} + \hat{C}^\dagger\hat{C})\hat{C} + i\Gamma\hat{B}^\dagger\hat{A}^2 + \sqrt{\alpha}\hat{c}_{\text{in}}, \tag{3}$$

where $\hat{A}$, $\hat{B}$, and $\hat{C}$ are the annihilation operators of the cavity modes for the pump, signal, and idler fields, respectively, α is the loss rate of the cavity, Δ_A, Δ_B, and Δ_C are the detunings of the pump, signal and idler modes, respectively, Γ is the cavity-enhanced nonlinear coefficient, κ is the input coupling rate, A_{in} is the input field as a c-number, and $\hat{a}_{\text{in}}$, $\hat{b}_{\text{in}}$, and $\hat{c}_{\text{in}}$ are the Langevin noise operators resulting from coupling to reservoirs with continuous mode spectra. We defined the detunings such that $\Delta_{A,B,C} > 0$ when the field is red detuned. The nonlinear coefficient can be expressed as,

$$\Gamma = \frac{3\hbar\omega_A^2\chi^{(3)}}{4\varepsilon_0 n_{\text{eff}}^2 n_g^2 V}, \tag{4}$$

where $\hbar$ is Planck's constant, ω_A is the pump angular frequency, $\chi^{(3)}$ is the Kerr nonlinear coefficient, ε_0 is the vacuum dielectric coefficient, n_{eff} is the effective index of the pump, n_g is the group index of the pump, and V is the mode volume. Since the vacuum fluctuations are much weaker than the mean photon numbers in the OPO state, we can linearize Eqs. (1) - (3) by rewriting the operators in terms of their mean values and fluctuations as,

$$\hat{O} = (O + \hat{u}_o + i\hat{v}_o)e^{i\phi_o}, \tag{5}$$

where $O \in \{A, B, C\}$. We choose the convention such that O is a positive number and $\hat{u}_o$ and $\hat{v}_o$ are Hermitian operators. Similarly, we expand $\hat{a}_{\text{in}}$, $\hat{b}_{\text{in}}$, and $\hat{c}_{\text{in}}$ as,

$$\hat{o}_{\text{in}} = \hat{g}_o + i\hat{h}_o, \tag{6}$$

where $o \in \{a, b, c\}$, and $\hat{g}_o$ and $\hat{h}_o$ are Hermitian operators satisfying the relations,

$$\langle\hat{g}_o(t)\hat{g}_o(t')\rangle = \langle\hat{h}_o(t)\hat{h}_o(t')\rangle = \frac{1}{4}\delta(t-t'), \tag{7}$$

$$\langle\hat{g}_o(t)\hat{h}_o(t')\rangle = \langle\hat{h}_o(t')\hat{g}_o(t)\rangle^* = \frac{i}{4}\delta(t-t'). \tag{8}$$

The operator equations after linearization reads,

$$\frac{d}{dt}\begin{pmatrix}\hat{u}_a\\ \hat{v}_a\\ \hat{u}_b\\ \hat{v}_b\\ \hat{u}_c\\ \hat{v}_c\end{pmatrix}=\mathbf{M}\begin{pmatrix}\hat{u}_a\\ \hat{v}_a\\ \hat{u}_b\\ \hat{v}_b\\ \hat{u}_c\\ \hat{v}_c\end{pmatrix}+\sqrt{\alpha}\begin{pmatrix}\hat{g}_a\\ \hat{h}_a\\ \hat{g}_b\\ \hat{h}_b\\ \hat{g}_c\\ \hat{h}_c\end{pmatrix}, \tag{9}$$

where $\mathbf{M}=\{m_{ij}\}_{6\times 6}$ with coefficients $m_{11}=-\frac{\alpha}{2}+2\Gamma BC\sin\phi$, $m_{12}=-\Gamma(A^2+2B^2+2C^2+2BC\cos\phi)+\Delta_A$, $m_{13}=2\Gamma AC\sin\phi$, $m_{14}=-2\Gamma AC\cos\phi$, $m_{15}=2\Gamma AB\sin\phi$, $m_{16}=-2\Gamma AB\cos\phi$, $m_{21}=\Gamma(3A^2+2B^2+2C^2+2BC\cos\phi)-\Delta_A$, $m_{22}=-\frac{\alpha}{2}-2\Gamma BC\sin\phi$, $m_{23}=\Gamma(4AB+2AC\cos\phi)$, $m_{24}=2\Gamma AC\sin\phi$, $m_{25}=\Gamma(4AC+2AB\cos\phi)$, $m_{26}=2\Gamma AB\sin\phi$, $m_{31}=-2\Gamma AC\sin\phi$, $m_{32}=-2\Gamma AC\cos\phi$, $m_{33}=-\frac{\alpha}{2}$, $m_{34}=-\Gamma(2A^2+B^2+2C^2)+\Delta_B$, $m_{35}=-\Gamma A^2\sin\phi$, $m_{36}=\Gamma A^2\cos\phi$, $m_{41}=\Gamma(4AB+2AC\cos\phi)$, $m_{42}=-2\Gamma AC\sin\phi$, $m_{43}=\Gamma(2A^2+3B^2+2C^2)-\Delta_B$, $m_{44}=-\frac{\alpha}{2}$, $m_{45}=\Gamma(4BC+A^2\cos\phi)$, $m_{46}=\Gamma A^2\sin\phi$, $m_{51}=-2\Gamma AB\sin\phi$, $m_{52}=-2\Gamma AB\cos\phi$, $m_{53}=-\Gamma A^2\sin\phi$, $m_{54}=\Gamma A^2\cos\phi$, $m_{55}=-\frac{\alpha}{2}$, $m_{56}=-\Gamma(2A^2+2B^2+C^2)+\Delta_C$, $m_{61}=\Gamma(4AC+2AB\cos\phi)$, $m_{62}=-2\Gamma AB\sin\phi$, $m_{63}=\Gamma(4BC+A^2\cos\phi)$, $m_{64}=\Gamma A^2\sin\phi$, $m_{65}=\Gamma(2A^2+2B^2+3C^2)-\Delta_C$, and $m_{66}=-\frac{\alpha}{2}$, where $\phi=2\phi_A-\phi_B-\phi_C$.

Equation (9) can be readily solved in the frequency domain with the Fourier transform,

$$\hat{o}(\omega)=\frac{1}{\sqrt{2\pi}}\int_{-\infty}^{\infty}\hat{o}(t)e^{i\omega t}dt, \tag{10}$$

where $o\in\{u_a,v_a,u_b,v_b,u_c,v_c,g_a,h_a,g_b,h_b,g_c,h_c\}$. The power spectral density of phase fluctuations of the signal can be evaluated as,

$$S(\omega)=\int\frac{\langle\hat{v}_b(\omega)\hat{v}_b(\omega')\rangle}{B^2}d\omega', \tag{11}$$

where $\hat{v}_b$ is a function of the frequency-domain noise operators satisfying,

$$\langle\hat{g}_o(\omega)\hat{g}_o(\omega')\rangle=\langle\hat{h}_o(\omega)\hat{h}_o(\omega')\rangle=\frac{1}{4}\delta(\omega-\omega'), \tag{12}$$

$$\langle\hat{g}_o(\omega)\hat{h}_o(\omega')\rangle=\langle\hat{h}_o(\omega')\hat{g}_o(\omega)\rangle^*=\frac{i}{4}\delta(\omega-\omega'). \tag{13}$$

In general, inverting $\mathbf{M}$ yields a complicated expression that needs to be evaluated numerically. However, in the current case where the signal and idler modes have identical loss rates, $\mathbf{M}$ can be simplified to yield a simple analytical approximation. First, we investigate the steady-state equations,

$$\frac{\alpha}{2}A+i\Delta_A A-i\Gamma(A^2+2B^2+2C^2)A-i2\Gamma ABCe^{-i\phi}=\sqrt{\kappa}A_{\text{in}}e^{-i\phi_A}, \tag{14}$$

$$\frac{\alpha}{2}B+i\Delta_B B-i\Gamma(2A^2+B^2+2C^2)B-i\Gamma A^2Ce^{i\phi}=0, \tag{15}$$

$$\frac{\alpha}{2}C+i\Delta_C C-i\Gamma(2A^2+2B^2+C^2)C-i\Gamma A^2Be^{i\phi}=0. \tag{16}$$

With some manipulation, we can find the following relations,

$$B=C, \tag{17}$$

$$\Delta_B=\Delta_C, \tag{18}$$

$$\Gamma A^2\sin\phi=-\frac{\alpha}{2}. \tag{19}$$

$$\Delta_B-\Gamma(2A^2+3B^2)=\Gamma A^2\cos\phi. \tag{20}$$

Furthermore, the typical STL of an OPO is much lower than the cavity linewidth. Using the relation between the phase-noise spectrum and laser linewidth [1], we find that only the lowest order of ω contributes to the linewidth. With some calculation, we can find these terms as,

$$\bar{v}_b=i\frac{\alpha[\hat{h}_c(\omega)-\hat{h}_b(\omega)]-2(\Delta_B-2\Gamma A^2-2\Gamma B^2)[\hat{g}_c(\omega)-\hat{g}_b(\omega)]}{2\sqrt{\alpha}\omega}. \tag{21}$$

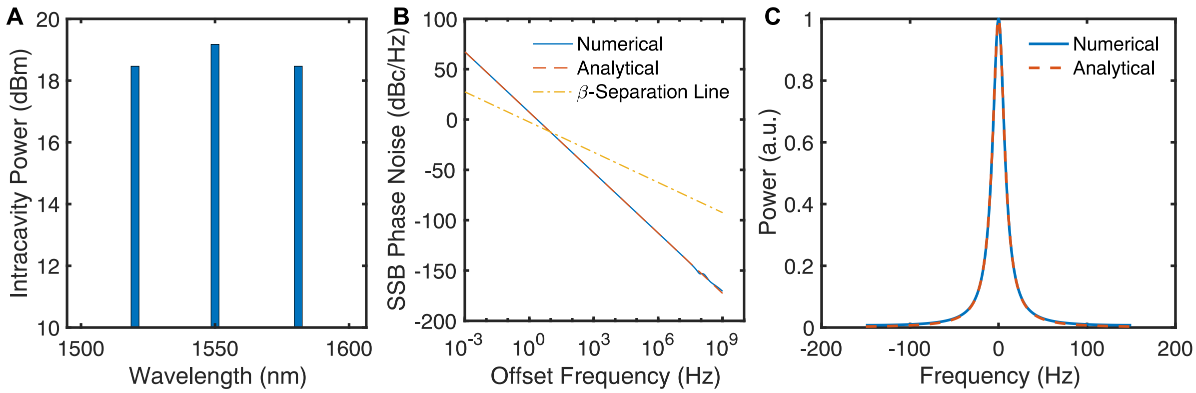

FIG. 1. Theory of Schawlow-Townes linewidth of $\chi^{(3)}$ OPO. (A) Intracavity optical spectrum in the 3-mode model. (B) Comparison of vacuum-fluctuation-limited phase noise between the numerical solution of Eq. (9) (blue trace) and the analytical solution of (23) (red trace). The β-separation line is also plotted, which indicates the part of phase noise that determines the laser linewidth. (C) The laser linewidth calculated by numerically integrating the blue trace in (B). The Lorentzian lineshape with an FWHM given in Eq. (24) is shown as the red trace.

Subsequently, we can find the phase-noise spectrum as,

$$S(\omega) = \frac{\alpha^2 + 4(\Delta_B - 2\Gamma A^2 - 2\Gamma B^2)^2}{4\alpha\omega^2 B^2}, \tag{22}$$

which correspond to the single-sideband (SSB) phase noise of,

$$\mathcal{L}(f) = \frac{\alpha^2 + 4(\Delta_B - 2\Gamma A^2 - 2\Gamma B^2)^2}{8\pi\alpha f^2 B^2}, \tag{23}$$

where f is the offset frequency. This represents a Brownian diffusion process that is found in many oscillator systems. The corresponding linewidth can be found as,

$$\Delta f_{\mathrm{ST}} = \frac{\hbar\omega_B\kappa\left[\alpha^2 + 4(\Delta_B - 2\Gamma A^2 - 2\Gamma B^2)^2\right]}{8\alpha P_B}, \tag{24}$$

where P_B is the output power of the signal with $P_B = \hbar\omega_B\kappa B^2$.

As an example, we simulate an OPO with $\alpha = 2\pi \times 200$ MHz, $\Delta_A = 2\pi \times 100$ MHz, and $\kappa = 2\pi \times 100$ MHz. We use 20 mW of pump power, corresponding to $|A_{\mathrm{in}}|^2 = 1.6 \times 10^{15}$ photons/s. In addition, we choose a free-spectral range of 200 GHz and a group-velocity dispersion (GVD) of -25 ps^2/km, corresponding to the OPO signal and idler at 1581.0 nm and 1520.2 nm, respectively, and $\Delta_B + \Delta_C - 2\Delta_A = 1.97$ GHz. The OPO optical spectrum is shown in Fig. 1A, where we have ignored the cascaded OPO lines due to their low powers. We numerically solve the phase-noise power spectrum using Eq. (9), which is shown as the blue trace in Fig. 1B. The analytical solution is plotted as the red trace, which only slightly deviates from the numerical solution at offset frequencies comparable to the cavity linewidth. The β-separation line has been used to identify the phase noise that contributes to laser linewidths [1], which is plotted in orange in Fig. 1B. The laser linewidth is primarily determined by the offset frequencies lower than the intersection point between the β-separation line and the noise spectrum, which is much lower than the cavity linewidth. This justifies our choice of keeping the lowest order of ω. The STL-limited OPO lineshape can be calculated numerically by integrating the blue trace in Fig. 1B [1], which is shown as the blue trace in Fig. 1C. The numerical result shows excellent agreement with a Lorentzian curve with full-width-at-half-maximum (FWHM) linewidth given by Eq. (24).

II. CLASSICAL NOISE SOURCES OF $\chi^{(3)}$-BASED OPO

The classical dynamics can be modeled analogously to the quantum dynamics of Eqs. (1)-(3). We use $\sim$ to indicate classical random processes, which yields the dynamical equations,

$$\frac{d\tilde{A}}{dt} = -\frac{\alpha}{2}\tilde{A} - i\tilde{\Delta}_A\tilde{A} + i\Gamma(\tilde{A}^*\tilde{A} + 2\tilde{B}^*\tilde{B} + 2\tilde{C}^*\tilde{C})\tilde{A} + i2\Gamma\tilde{A}^*\tilde{B}\tilde{C} + \sqrt{\kappa}\tilde{A}_{\text{in}}, \tag{25}$$

$$\frac{d\tilde{B}}{dt} = -\frac{\alpha}{2}\tilde{B} - i\tilde{\Delta}_B\tilde{B} + i\Gamma(2\tilde{A}^*\tilde{A} + \tilde{B}^*\tilde{B} + 2\tilde{C}^*\tilde{C})\tilde{B} + i\Gamma\tilde{C}^*\tilde{A}^2, \tag{26}$$

$$\frac{d\tilde{C}}{dt} = -\frac{\alpha}{2}\tilde{C} - i\tilde{\Delta}_C\tilde{C} + i\Gamma(2\tilde{A}^*\tilde{A} + 2\tilde{B}^*\tilde{B} + \tilde{C}^*\tilde{C})\tilde{C} + i\Gamma\tilde{B}^*\tilde{A}^2, \tag{27}$$

where $\tilde{A}$, $\tilde{B}$, and $\tilde{C}$ are the field amplitudes normalized to photon number in the cavity, $\tilde{\Delta}_A$, $\tilde{\Delta}_B$, and $\tilde{\Delta}_C$ are the (fluctuating) detunings of the pump, signal, and idler fields, respectively, and A_{in} is the pump field in the bus waveguide normalized to photon flux. All the other parameters follow the definition in section I. We can similarly decompose the fields into their mean and fluctuating parts as,

$$\tilde{O} = (O + \tilde{u}_o + i\tilde{v}_o)e^{i\phi_o}, \tag{28}$$

where $O \in \{A, B, C\}$. A, B, and C correspond to the average amplitude of the fields, $\tilde{u}_a/A$, $\tilde{u}_b/B$, and $\tilde{u}_c/C$ correspond to the relative amplitude noise, and $\tilde{v}_a/A$, $\tilde{v}_b/B$, and $\tilde{v}_c/C$ correspond to the phase noise. In addtiona, we let $\tilde{A}_{\text{in}} = (A_{\text{in}} + \tilde{u}_{\text{in}} + i\tilde{v}_{\text{in}})$ and $\tilde{\Delta}_{A,B,C} = \Delta_{A,B,C} + \tilde{\delta}_{a,b,c}$. The mean values follow the same equations as Eq. (14)-(16). Using Eq. (17)-(19) and with some calculation, we can find the difference of signal idler fluctuations as,

$$\frac{d}{dt}(\tilde{u}_b - \tilde{u}_c) = -\alpha(\tilde{u}_b - \tilde{u}_c), \tag{29}$$

$$\frac{d}{dt}(\tilde{v}_b - \tilde{v}_c) = -(\tilde{\delta}_b B - \tilde{\delta}_c C) - 2\left(BC + A^2\cos\phi\right)(\tilde{u}_b - \tilde{u}_c), \tag{30}$$

where $\phi = 2\phi_A - \phi_B - \phi_C$, and we have used Eqs. (17) - (20). Equation (29) indicates $\tilde{u}_b = \tilde{u}_c$ as the amplitude damps without a driving force, which physically corresponds to energy conservation. Thus, using Eq. (30), we get the phase difference as,

$$\frac{d}{dt}(\tilde{\phi}_b - \tilde{\phi}_c) = -(\tilde{\delta}_b - \tilde{\delta}_c). \tag{31}$$

Equations (25) - (27) can also be directly simulated. To generate Fig. 2A in the main text, we use the same cavity parameters as those in Fig. 1. We assume the detuning noise follows $\tilde{\delta}_x = k_x\tilde{t}$, where $x \in \{A, B, C\}$, k_A, k_B, k_C are constant coefficients, and $\tilde{t}$ is the temperature fluctuation identical to ΔT in the main text. In addition, we let

$$k_A : k_B : k_C = \omega_A : \omega_B : \omega_C, \tag{32}$$

and characterize $k_A\tilde{t}$ using the method in section **??**.

III. NUMERICAL MODEL OF SYNCHRONIZATION

The model of OPO-soliton synchronization is identical to that for the soliton-soliton synchronization presented in [2], which we list here as,

$$\frac{\partial E_1}{\partial t} = \left(-\frac{\alpha}{2} - i\Delta_1 - i\frac{L\mathcal{F}\beta_2}{2}\frac{\partial^2}{\partial\tau^2} + i\gamma L\mathcal{F}|E_1|^2\right)E_1 + \sqrt{\kappa\mathcal{F}}E_{\text{in},1}, \tag{33}$$

$$\frac{\partial E_2}{\partial t} = \left(-\frac{\alpha}{2} - i\Delta_2 - \tau_d\mathcal{F}\frac{\partial}{\partial\tau} - i\frac{L\mathcal{F}\beta_2}{2}\frac{\partial^2}{\partial\tau^2} + i\gamma L\mathcal{F}|E_2|^2\right)E_2 + \sqrt{\kappa\mathcal{F}}E_{\text{in},2} + \theta\mathcal{F}E_1, \tag{34}$$

where E_1 and E_2 are the field envelope in the OPO and soliton-comb cavities, respectively, α is the cavity loss rate, Δ_1 and Δ_2 are the pump detunings of the OPO and soliton-comb cavities, respectively, τ_d is the difference of the roundtrip time between the cavities, L is the roundtrip length, $\mathcal{F}$ is the free-spectral range (FSR), β_2 is the GVD

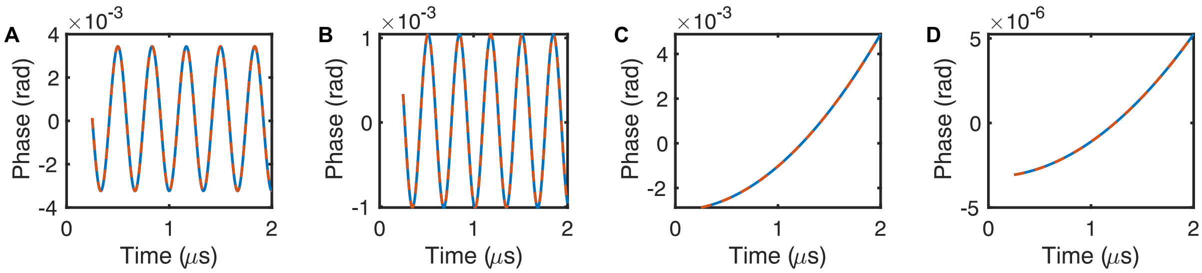

FIG. 2. Characterization of noise suppression via synchronization. (A-D), The repetition-rate change induced by a sinusoidal modulation of τ_d at a frequency of 3 MHz (A, B) and 10 kHz (C, D) without the coupling link (A, C) and with the coupling link (B, D), where the scale of the vertical axes are vastly different. The solid traces are numerical simulations with Eqs. (33) and (34), and the dashed traces are sinusoidal fits. Even though the simulation time is less than one period of the 10-kHz oscillation, the fit is sufficient to recover the amplitude of the phase fluctuation.

coefficient, γ is the nonlinear coefficient, κ is the pump coupling rate, θ is the roundtrip coupling coefficient of the coupling link at each coupling point, $E_{\text{in},1}$ and $E_{\text{in},2}$ are the input pump fields of the OPO and soliton cavities, respectively, t is the slow time on the scale of cavity lifetime, and τ is the fast time on the scale of cavity roundtrip time. Unlike the previous sections, all the fields in this section are normalized to power. We have ignored the time delay introduced by the coupling link, which can be incorporated with a frequency-dependent phase term for θ.

The field evolution can be simulated using the split-step Fourier method. We use $\alpha = 2\pi \times 200$ MHz, $\kappa = 2\pi \times 100$ MHz, $\beta_2 =$ -25 ps^2/km, $\mathcal{F} = 200$ GHz, and $L = 2\pi \times 110\mu$m, which is identical to those in section I. We use a pump power of 20 mW and detuning of $2\pi \times 50$ MHz for the OPO, and a pump of 100 mW and a detuning of $2\pi \times 800$ MHz for the soliton. To demonstrate roundtrip-time synchronization, we set a roundtrip-time difference $\tau_d = 0.02$ fs, which is shown as a drift on the fast-time grid (Fig. 2E in the main text). This drift is stopped by introducing a coupling $\theta = 0.15\%$, corresponding to a total power coupling of $\theta^2 = 2.25 \times 10^{-6}$ in a roundtrip time.

We simulate the suppression of soliton noise by introducing a sinusoidal modulation in τ_d, which results in a sinusoidal change of soliton-repetition rate. We read out this change by extracting the phase of the comb line next to the pump, as the phase of the pump mode is constant for all τ_d. We then fit the comb line phase with a sine function to extract the modulation amplitude. By comparing the amplitude with $\theta = 0$ and $\theta \neq 0$, we can get the maximum noise suppression strength at a given offset frequency. This method avoids propagation for a long time at small offset frequencies. We simulate variations at frequencies 1 kHz, 3 kHz, 10 kHz, 30 kHz, $\cdots$, 300 MHz, and 1 GHz, and show typical results in Fig. 2. The noise suppression factor at an offset frequency is the ratio between the amplitudes with and without synchronization, which reflects the maximum noise-rejection capability when the OPO noise is much lower than the soliton noise. If the OPO noise is above the soliton noise minus the noise-suppression factor, the soliton noise follows the OPO noise after synchronization.

IV. LOW-THERMOREFRACTIVE-NOISE DESIGN

As shown in Eq. (3), the thermorefractive noise in OPA corresponds to the mismatch between the resonance shift of the signal and the idler caused by temperature fluctuations. The resonance frequency ω satisfies

$$\frac{n_{\text{eff}}\omega L}{c} = 2\pi m, \tag{35}$$

where n_{eff} is the effective index, L is the cavity length, c is the speed of light in vacuum, and m is the resonator mode number. Differentiating Eq. (35) with respect to the temperature T, we can get the resonance-shift coefficient,

$$k = \frac{d\omega}{dT} = \frac{\omega}{n_g}\frac{dn_{\text{eff}}}{dT}, \tag{36}$$

where n_g is the group index. In a regular silicon-nitride (SiN) waveguide, ω is the dominant term, and k increases as the frequency increases. However, by incorporating a small amount of TiO_2, which has a thermorefractive coefficient of -1$\times 10^{-4}$ K^{-1}, we can significantly reduce dn_{eff}/dT, and increase its slope as a function of wavelength. Fig. 3A shows an example of such a structure. A 100-nm thick TiO_2 layer is placed 50 nm away from the (SiN) core, which allows good mode confinement. We simulate the effective index at different wavelengths and temperatures using

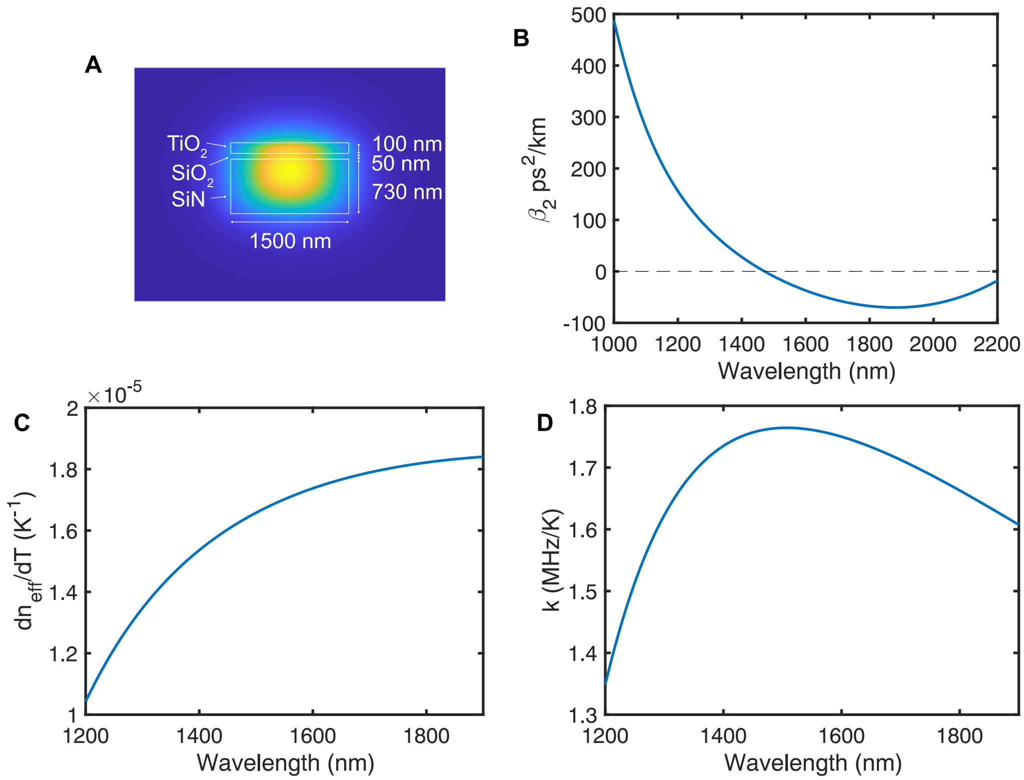

FIG. 3. Design of a waveguide with tailored thermal properties for low-noise OPO. (A), the structure and simulated mode profile of the waveguide. (B), the simulated GVD of the waveguide. (C), The simulated thermorefractive coefficient of the waveguide. (D), The thermal-induced resonance shift as a function of wavelength, showing pairs of wavelengths with identical shift coefficients at the telecom wavelengths.

the thermorefractive coefficient for SiN as 0.4×10^{-4} K^{-1} and SiO_2 as 0.1×10^{-4} K^{-1}. As shown in Fig. 3B, the waveguide exhibits anomalous GVD around 1550 nm. The effective index has a non-zero themorefractive coefficient which increases as a function of wavelength. This allows pairs of wavelengths with identical k coefficients, which can be used to suppress the thermal noise in OPO operation.

* a.gaeta@columbia.edu

[1] G. D. Domenico, S. Schilt, and P. Thomann, Simple approach to the relation between laser frequency noise and laser line shape, Appl. Opt. **49**, 4801 (2010).

[2] J. K. Jang, A. Klenner, X. Ji, Y. Okawachi, M. Lipson, and A. L. Gaeta, Synchronization of coupled optical microresonators, Nat. Photonics **12**, 688 (2018).